Inorganic Chemistry

Article

pubs.acs.org/IC

Flux Growth of $Yb_{6.6}Ir_6Sn_{16}$ Having Mixed-Valent Ytterbium

Sebastian C. Peter,*[,†] Udumula Subbarao,[†] Sudhindra Rayaprol,[‡] Joshua B. Martin,[§] Mahalingam Balasubramanian,[∥] Christos D. Malliakas,[⊥,⊗] and Mercouri G. Kanatzidis*[,⊥,⊗]

[†]New Chemistry Unit, Jawaharlal Nehru Centre for Advanced Scientific Research, Jakkur, Bangalore 560064, India

[‡]UGC-DAE Consortium for Scientific Research, Mumbai Centre, BARC, R-5 Shed, Trombay, Mumbai 400085, India

[§]Material Measurement Laboratory, National Institute of Standards and Technology (NIST), 100 Bureau Drive, Stop 8520, Gaithersburg, Maryland 20899, United States

[∥]Advanced Photon Source, Argonne National Laboratory, Argonne, Illinois 60439, United States

[⊥]Department of Chemistry, Northwestern University, 2145 N. Sheridan Road, Evanston, Illinois 60208, United States

[⊗]Materials Science Division, Argonne National Laboratory, Argonne, Illinois 60439, United States

Supporting Information

ABSTRACT: The compound $Yb_{6.6}Ir_6Sn_{16}$ was obtained as single crystals in high yield from the reaction of Yb with Ir and Sn run in excess indium. Single-crystal X-ray diffraction analysis shows that $Yb_{6.6}Ir_6Sn_{16}$ crystallizes in the tetragonal space group $P4_2/nmc$ with $a = b = 9.7105(7)$ Å and $c = 13.7183(11)$ Å. The crystal structure is composed of a $[Ir_6Sn_{16}]$ polyanionic network with cages in which the Yb atoms are embedded. The Yb sublattice features extensive vacancies on one crystallographic site. Magnetic susceptibility measurements on single crystals indicate Curie–Weiss law behavior <100 K with no magnetic ordering down to 2 K. The magnetic moment within the linear region (<100 K) is 3.21 μ_B/Yb, which is ~70% of the expected value for a free Yb^{3+} ion suggesting the presence of mixed-valent ytterbium atoms. X-ray absorption near edge spectroscopy confirms that $Yb_{6.6}Ir_6Sn_{16}$ exhibits mixed valence. Resistivity and heat capacity measurements for $Yb_{6.6}Ir_6Sn_{16}$ indicate non-Fermi liquid metallic behavior.

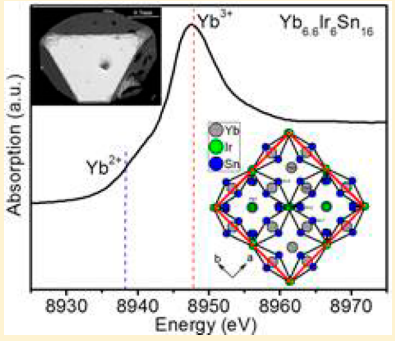

1. INTRODUCTION

Rare earth (*RE*) iridium stannides are an interesting class of materials because of their structural diversity and unusual physical properties. The compounds reported in this family include: *RE*IrSn (*RE* = La–Pr, Sm, Eu–Tb, Ho–Lu), which crystallize in the ZrNiAl structure type and the $P\bar{6}2m$ space group;[1−3] $CeIr_2Sn_2$, which adopts the tetragonal $CaBe_2Ge_2$ structure type with $P4/nmm$ space group;[4] $MgCuAl_2$-type $EuIrSn_2$ ($Cmcm$ space group);[5] $REIr_xSn_2$ (*RE* = La, Nd, Gd) in the $CeNiSi_2$ structure type and $Cmmm$ space group;[6] $RE_3Ir_4Sn_{13}$ (*RE* = La–Pr, Sm, Eu, Er–Lu), which adopt the cubic $Yb_3Rh_4Sn_{13}$ structure type ($Pm\bar{3}n$ space group);[7,8] and $RE_5Ir_4Sn_{10}$ (*RE* = La–Pr), which adopt the $Sc_5Co_4Si_{10}$ structure with $P4/mbm$ space group.[9] Apart from the above-mentioned compounds, Espinosa and Cooper reported the tin-rich family $RE_5T_{5.5}Sn_{18}$ consisting of an *RE* or other metal such as Ca, Sr, or Th with the transition metals Co, Ru, Rh, and Ir.[10,11] Considerable attention has also been paid to compounds where T is a late second or third row transition metal such as Rh, Ir, or Ru, which exhibit superconducting and/or interesting magnetic properties.[10,11] Among them, $Yb_5Ir_{5.5}Sn_{18}$ is the most interesting because of its structural diversity. The early work of Espinosa using powder X-ray diffraction (XRD) has pointed to at least five different structures, deriving from compositional variations created by the nonequilibrium conditions during synthesis. The observed phases were primitive cubic, tetragonal, face centered cubic, slightly distorted body centered cubic [Ir_3Sn_7 structure type], and an unidentified phase as well.[10]

The structural diversity of the $Yb_5Ir_{5.5}Sn_{18}$ compound and our continued interest in ytterbium-based intermetallic compounds,[12−31] which is based on the valence flexibility of ytterbium, allowing it to adopt different or mixed oxidation states,[32−35] motivates our current work. The presence of an unstable electronic 4*f* shell can cause the Yb ion to show two electronic configurations that are closely spaced in energy: the magnetic Yb^{3+} ($4f^{13}$) and the nonmagnetic Yb^{2+} ($4f^{14}$). It is generally believed that the stability of the different ground states depends strongly on the hybridization (interaction) strength between the magnetic 4*f* electrons and the *s*, *p*, and *d* conduction electrons.[33,36,37] Mixed valence in Yb atoms can give rise to the Kondo effect or heavy-Fermion behavior.[38−42] During our investigations of the $Yb_5Ir_{5.5}Sn_{18}$ compound we discovered the compound $Yb_{6.6}Ir_6Sn_{16}$.

Here, we report the synthesis of $Yb_{6.6}Ir_6Sn_{16}$ using the indium-flux method. Single-crystal XRD analysis revealed that $Yb_{6.6}Ir_6Sn_{16}$ crystallizes in tetragonal structure type. The magnetic and X-ray absorption near edge spectroscopy (XANES) studies suggest that $Yb_{6.6}Ir_6Sn_{16}$ has mixed valency in its Yb atoms. Resistivity and heat capacity measurements for

Received: January 27, 2014
Published: June 12, 2014

   dx.doi.org/10.1021/ic500204t | *Inorg. Chem.* 2014, 53, 6615−6623

$Yb_{6.6}Ir_6Sn_{16}$ indicate non-Fermi liquid metallic behavior and confirm the absence of magnetic ordering down to 2 K.

2. EXPERIMENTAL SECTION

2.1. Synthesis. The following reagents were used as purchased without further purification: Yb (metal chunk, 99.9%, Chinese Rare Earth Information Center, China), Ir (pieces, 99.9%, Alfa Aesar, Ward Hill, MA), Sn (pieces, 99.9%, Alfa Aesar, Ward Hill, MA), and In (tear drops 99.99%, Plasmaterials, Livermore, CA). The purpose of identifying the equipment in this article is to specify the experimental procedure. Such identification does not imply recommendation or endorsement by the National Institute of Standards and Technology.

2.1.1. Metal Flux Method. Well-shaped single crystals of $Yb_{6.6}Ir_6Sn_{16}$ were obtained by combining 3 mmol of Yb, 2 mmol of Ir, 6 mmol of Sn, and 30 mmol of In in an Al_2O_3 crucible, which was then flame-sealed under a reduced-pressure atmosphere of 10^{-4} mbar in a fused silica tube. The reactants were then heated to 1000 °C over 10 h, maintained at that temperature for 5 h to allow proper homogenization, followed by cooling to 850 °C in 2 h, and held there for 48 h. Finally, the sample was allowed to slowly cool to 50 °C in 48 h. The reaction product was isolated from the excess indium flux by heating at 350 °C and subsequently centrifuging through a coarse frit. Any remaining flux was removed by immersion and sonication in glacial acetic acid for 48 h. The final crystalline product was rinsed with water and dried with acetone. This method produced the target compound in well-shaped crystals and in a large yield, more than 95% on the basis of the initial amount of Yb metal used in the reaction. Crystals of $Yb_{6.6}Ir_6Sn_{16}$ grow as well-formed prisms that are metallic silver in appearance sizes of ~3.0 × 2.0 × 2.0 mm.

2.1.2. Synthesis of $Yb_{6.6}Ir_6Sn_{16}$ Using High-Frequency Induction Heating. Ytterbium, iridium, and tin elements were mixed in the ideal 6.6:6:16 atomic ratio and sealed in a tantalum ampule under argon atmosphere in an arc-melting apparatus. The tantalum ampule was subsequently placed in a water-cooled sample chamber of an induction furnace (Easy Heat induction heating system, Model 7590), first rapidly heated to 180 Amperes (ca. 1200−1350 K) and kept at that temperature for 30 min. Finally, the reaction was rapidly cooled to room temperature by switching off the power supply. The light gray compound could easily be removed in polycrystalline form from the tantalum tube. No reactions with the crucible material could be detected. Yield was 95% on the basis of the initial amount of Yb metal used in the reaction, and the sample was pure, with no secondary crystalline phases present within the detection limit of in-house XRD. $Yb_{6.6}Ir_6Sn_{16}$ is stable in moist air for several months. The sample obtained from the high-frequency induction heating method was used for the resistivity studies.

2.2. Elemental Analysis. Quantitative microprobe analyses of $Yb_{6.6}Ir_6Sn_{16}$ were performed with a Hitachi S-3400 scanning electron microscope (SEM) equipped with a PGT energy dispersive X-ray analyzer (EDS). Data were acquired with an accelerating voltage of 20 kV and a 60 s accumulation time. The EDS analyses taken on visibly clean surfaces of the $Yb_{6.6}Ir_6Sn_{16}$ crystals gave the atomic composition of 23(±1)% Yb, 21(±1)% Ir, and 56(±1)% Sn, which is in good agreement with the results derived from the single-crystal XRD refinements.

2.3. Powder X-ray Diffraction. Phase identity and purity of $Yb_{6.6}Ir_6Sn_{16}$ was determined by powder XRD experiments that were carried out on an Inel diffractometer using Cu Kα radiation. Experimental powder patterns were compared to patterns calculated from the structural refinement. The powder XRD pattern of $Yb_{6.6}Ir_6Sn_{16}$ was in good agreement with the simulated pattern.

2.4. Single-Crystal X-ray Diffraction. The X-ray intensity data were collected at room temperature using a STOE IPDS 2T (with additional capability of 2θ swing of the detector) diffractometer with graphite-monochromatized Mo Kα (λ = 0.710 73 Å) radiation. The X-AREA (X-RED and X-SHAPE) package suite[43] was used for the data extraction and integration and to apply empirical and analytical absorption corrections. The crystal structure of $Yb_{6.6}Ir_6Sn_{16}$ was refined with the JANA2006[44] package of programs. The unit cell edge length determination was performed with the Peak list 1.06 software part of the X-Area 1.39 suite[43] using a least-squares refinement algorithm.

2.5. Structure Refinement. In the first step, the intense peaks in the powder XRD pattern of $Yb_{6.6}Ir_6Sn_{16}$ were considered and suggested that the compound crystallizes in the $Tb_5Rh_6Sn_{17}$ structure type.[45] The single-crystal data of $Yb_{6.6}Ir_6Sn_{16}$ also showed a cubic cell, and the systematic extinctions were compatible with the space group $F\bar{4}3m$. Therefore, the atomic parameters of $Tb_5Rh_6Sn_{17}$ were taken as starting points to refine the structure using JANA2006[44] with anisotropic atomic displacement parameters for all atoms. As a check for the correct composition, the occupancy parameters were refined in a separate series of least-squares cycles. Similar to $Tb_5Rh_6Sn_{17}$, seven crystallographically different positions were found in the $Yb_{6.6}Ir_6Sn_{16}$ structure—two Yb atoms, one Ir atom, and four Sn atoms. During isotropic refinement it was observed that the atomic displacement parameters of the Sn3 atoms were anomalously large (109(7) Å^2 × 10^3). Furthermore, the refinement was largely unsatisfactory, giving relatively high residuals (R_1 > 19%) and large electron density residuals (48−20 eÅ^{-3}) around the Ir and Sn atoms. The anomalous atomic displacement parameter could not be resolved by subsequent refinement of the occupancy parameters. All these features suggest crystallographic disorder associated with the Ir and Sn atoms. An attempt to mix with Ir and Sn atoms also did not improve the refinement of the structure in cubic $F\bar{4}3m$ space group. To resolve this, the weak reflections (Figure 1) were also considered, and a stable

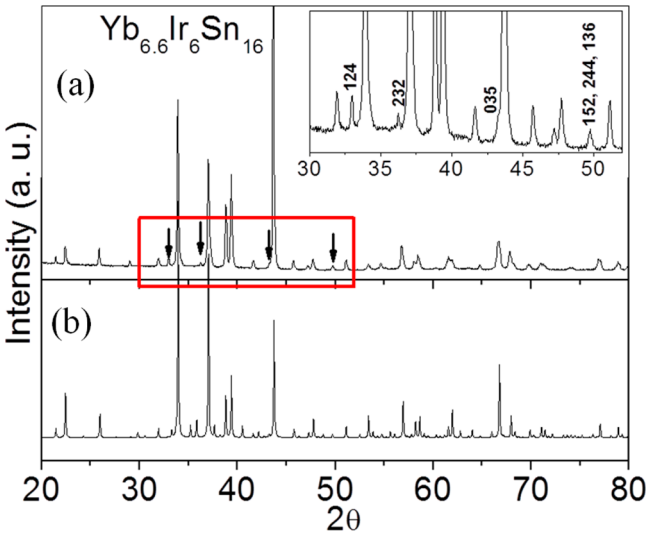

Figure 1. Experimental powder XRD pattern of $Yb_{6.6}Ir_6Sn_{16}$ (a) compared with the simulated pattern obtained from the single-crystal XRD structure refinement (b). (inset) The expanded view marked with *hkl* indices corresponds to weak reflections in the tetragonal structure.

refinement for $Yb_{6.6}Ir_6Sn_{16}$ in the tetragonal space group $P4_2/mnc$ was accomplished. Even in the $P4_2/mnc$ refinement, disorder still exists in the Yb(3) site in the form of partial occupancy and a large isotropic displacement parameter. The details of the data collection and crystallographic refinement of $Yb_{6.6}Ir_6Sn_{16}$ are given in Table 1. A list of the atomic positions, the isotropic displacement parameters, the anisotropic displacement parameters, and the bond distances are available in Tables 2−4. There is no direct subgroup−supergroup relationship between $P4_2/nmc$ ($Yb_{6.6}Sn_6Sn_{16}$) and $F\bar{4}3m$ ($Tb_5Rh_6Sn_{17}$). Given the systematic reflections observed in our diffraction data that violate the $F\bar{4}3m$ spacegroup and the disordered Yb(3) site, we believe the previously reported $Yb_5Sn_{5.5}Sn_{18}$ structure may be a partially ordered variant of $Tb_5Rh_6Sn_{17}$ but still an average structure of a possible Yb/vacancy ordered superstructure that is not yet resolved at the temperature of the data collection.

dx.doi.org/10.1021/ic500204t | Inorg. Chem. 2014, 53, 6615−6623

Table 1. Crystal Data and Structure Refinement for $Yb_{6.6}Ir_6Sn_{16}$ at 100(2) K

empirical formula	$Yb_{6.6}Ir_6Sn_{16}$
formula weight	4187.1 g/mol
temperature	100(2) K
wavelength	0.710 73 Å
crystal system	tetragonal
space group	$P4_2/nmc$
unit cell dimensions	$a = b = 9.7105(7)$ Å
	$c = 13.7183(11)$ Å
volume	1293.55(17) Å^3
Z	2
density (calculated)	10.76 g/cm^3
absorption coefficient	69.38 mm^{-1}
$F(000)$	3444
crystal size	0.080 × 0.061 × 0.046 mm^3
θ range for data collection	2.57 to 29.14°
index ranges	$-13 \le h \le 13$, $-11 \le k \le 12$, $-18 \le l \le 18$
reflections collected	9584
independent reflections	949 [$R_{int} = 0.0506$]
refinement method	full-matrix least-squares on F^2
data/restraints/parameters	949/0/47
goodness-of-fit	3.11
final R indices [$>2\sigma(I)$][a]	$R_{obs} = 0.0636$, $wR_{obs} = 0.1499$
R indices [all data]	$R_{all} = 0.0699$, $wR_{all} = 0.1568$
extinction coefficient	2200(300)
largest diff. peak and hole	4.35 and −3.62 e·Å^{-3}

[a] $R = \Sigma||F_o| - |F_c||/\Sigma|F_o|$, $wR = \{\Sigma[w(|F_o|^2 - |F_c|^2)^2]/\Sigma[w(|F_o|^4)]\}^{1/2}$, and $w = 1/(\sigma^2(I) + 0.0016I^2)$.

Table 2. Atomic Coordinates (× 10^4) and Equivalent Isotropic Displacement Parameters (Å^2 × 10^3) for $Yb_{6.6}Ir_6Sn_{16}$ at 100(2) K with Estimated Standard Deviations in Parentheses

label	x	y	z	occupancy	U_{eq}[a]
Yb(1)	2500	7500	2500	1	6(1)
Yb(2)	4860(2)	2500	1180(1)	1	2(1)
Yb(3)	2500	2874(6)	9819(4)	0.393(9)	36(2)
Ir(1)	7500	2500	88(1)	1	2(1)
Ir(2)	5088(1)	88(1)	2500	1	2(1)
Sn(1)	7500	637(2)	1568(2)	1	4(1)
Sn(2)	5794(2)	4295(2)	9250(1)	1	5(1)
Sn(3)	2500	1002(2)	2576(2)	1	3(1)

[a] U_{eq} is defined as one-third of the trace of the orthogonalized U_{ij} tensor.

Table 3. Anisotropic Displacement Parameters (Å^2 × 10^3) for $Yb_{6.6}Ir_6Sn_{16}$ at 100(2) K with Estimated Standard Deviations in Parentheses

label	U_{11}[a]	U_{22}[a]	U_{33}[a]	U_{12}[a]	U_{13}[a]	U_{23}[a]
Yb(1)	5(1)	5(1)	7(1)	0	0	0
Yb(2)	2(1)	1(1)	3(1)	0	0(1)	0
Yb(3)	48(4)	23(4)	37(4)	0	0	5(2)
Ir(1)	2(1)	1(1)	2(1)	0	0	0
Ir(2)	2(1)	2(1)	2(1)	0(1)	0(1)	0(1)
Sn(1)	4(1)	5(1)	3(1)	0	0	2(1)
Sn(2)	4(1)	7(1)	4(1)	2(1)	−2(1)	0(1)
Sn(3)	2(1)	3(1)	3(1)	0	0	2(1)

[a] The anisotropic displacement factor exponent takes the form: $-2\pi^2[h^2a^{*2}U_{11} + ... + 2hka^*b^*U_{12}]$.

2.6. Physical Properties. Magnetic measurements of $Yb_{6.6}Ir_6Sn_{16}$ as a function of temperature (magnetic susceptibility) were carried out on a Quantum Design MPMS-SQUID magnetometer. The resistivity measurements were performed in zero field in the range of 3−300 K with a conventional alternating current four probes setup using a commercial Quantum Design Physical Property Measurement System (QD-PPMS). Four very thin copper wires were glued to the pellet using a strongly conducting silver epoxy paste. Temperature-dependent heat capacity (C_p) of $Yb_{6.6}Ir_6Sn_{16}$ was measured in the range of 5−300 K using a QD-PPMS. The data were obtained using standard thermal relaxation methods in a zero magnetic field. Thermal coupling between the sample and the sample platform was enhanced with Apiezon N grease, and the sample platform coupled to the sample puck via thin wires. Conduction through these wires is the dominant mode of thermal transfer, enabled by cryopumping the chamber to less than 1.3 × 10^{-5} Pa. Prior to each sample measurement, the sample puck, platform, and the Apiezon N grease were thoroughly characterized in a separate addenda measurement. The uncertainty in the heat capacity measurements is less than 1% throughout the measured temperature range.

2.7. X-ray Absorption Near-Edge Spectroscopy. XANES experiments were performed at the Sector 20 bending magnet beamline (PNC/XSD, 20-BM) of the Advanced Photon Source at the Argonne National Laboratory. Measurements at the Yb L_{III} edge were performed in the transmission mode using gas ionization chambers to monitor the incident and transmitted X-ray intensities. A third ionization chamber was used in conjunction with a copper foil to provide internal calibration for the alignment of the edge positions. Monochromatic X-rays were obtained using a Si (111) double crystal monochromator. The monochromator was calibrated by defining the inflection point (first derivative maxima) of Cu foil as 8980.5 eV. A Rh-coated X-ray mirror was utilized to suppress higher-order harmonics. XANES samples were prepared by mixing an appropriate amount of the finely ground $Yb_{6.6}Ir_6Sn_{16}$ with BN. The mixture was pressed to form a self-supporting pellet, and the measurements were performed at 300 K. Care was taken to suppress distortion in the data from thickness effects.

dx.doi.org/10.1021/ic500204t | Inorg. Chem. 2014, 53, 6615−6623

Table 4. Selected Bond Lengths [Å] for $Yb_{6.6}Ir_6Sn_{16}$ at 100(2) K with Estimated Standard Deviations in Parentheses

label	distance	label	distance
Yb(1)−Sn(2) × 8	3.3978(16)	Yb(3)−Sn(3) × 2	3.422(6)
Yb(1)−Sn(3) × 4	3.4024(19)	Ir(1)−Sn(1) × 2	2.720(2)
Yb(2)−Yb(3) × 2	2.979(4)	Ir(1)−Sn(2) × 4	2.6655(19)
Yb(2)−Ir(1)	2.9695(15)	Ir(2)−Sn(1) × 2	2.7204(12)
Yb(2)−Ir(2) × 2	2.9681(9)	Ir(2)−Sn(2) × 2	2.6628(14)
Yb(2)−Sn(1) × 3	3.1825(18)	Ir(2)−Sn(3) × 2	2.6676(10)
Yb(2)−Sn(2) × 2	3.2978(18)	Sn(2)−Sn(2)	2.913(2)
Yb(2)−Sn(2) × 2	3.231(2)	Sn(2)−Sn(2)	3.486(3)
Yb(2)−Sn(3) × 2	3.322(2)	Sn(2)−Sn(2)	3.313(3)
Yb(3)−Yb(3)	0.727(8)	Sn(2)−Sn(3)	3.369(2)
Yb(3)−Sn(1)	3.289(6)	Sn(2)−Sn(3)	3.431(2)
Yb(3)−Sn(2) × 2	3.454(5)	Sn(3)−Sn(3)	2.909(3)

3. RESULTS AND DISCUSSION

3.1. Reaction Chemistry. The tetragonal phase of $Yb_{6.6}Ir_6Sn_{16}$ was synthesized in high yield from a reaction of ytterbium, iridium, tin, and excess indium. The truncated cube-shaped single crystals were silver metallic in color and up to 3 mm × 2 mm × 2 mm in size. They were stable in air, and no decomposition was observed even after several months. Attempts to change the amount of tin in the reaction to look for other phases proposed by Espinosa and Cooper also resulted in the $Yb_{6.6}Ir_6Sn_{16}$ tetragonal phase, although extensive studies in this direction were not carried out. An SEM image of a typical polyhedral crystal of $Yb_{6.6}Ir_6Sn_{16}$ grown from the flux synthesis is shown in Figure 2. Small amounts of $YbIrIn_2$ and

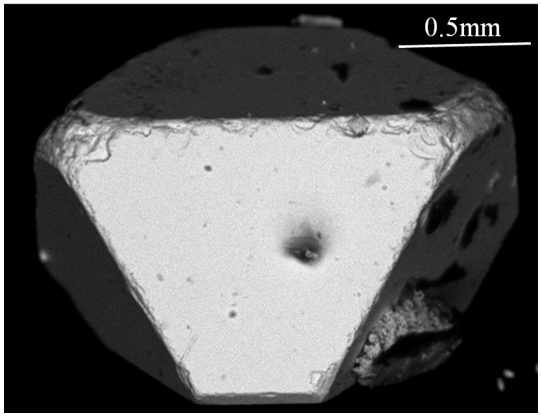

Figure 2. SEM image of typical single crystals of $Yb_{6.6}Ir_6Sn_{16}$.

residual In metal were also found in the reaction mixture. High-frequency induction heating of a stoichiometric mixture of the elements was also successful in producing the title compound.

3.2. Crystal Chemistry. The structure of $Yb_{6.6}Ir_6Sn_{16}$ is composed of a complex three-dimensional $[Ir_6Sn_{16}]$ polyanionic network with cages hosting the Yb atoms, Figure 3. These polyhedral cages share edges defined by Ir and Sn atoms. Cooper observed five different phases in the Yb−Ir−Sn family: (a) primitive cubic, $P\bar{4}3m$ or $Pm\bar{3}n$ space group (a = 9.709 Å), (b) face-centered cubic, $F\bar{4}3m$ space group (a = 13.751 Å), (c) tetragonal (a = 13.757 Å, c = 9.703 Å), (d) a phase crystallizing in lower symmetry closely related to the Ir_3Sn_7 type structure, and (e) an unknown phase.[11] In the present work, we refined the crystal structure of $Yb_{6.6}Ir_6Sn_{16}$ within the tetragonal system. By considering the fact that the lattice constants of the tetragonal system are related to the cubic lattice constants by a

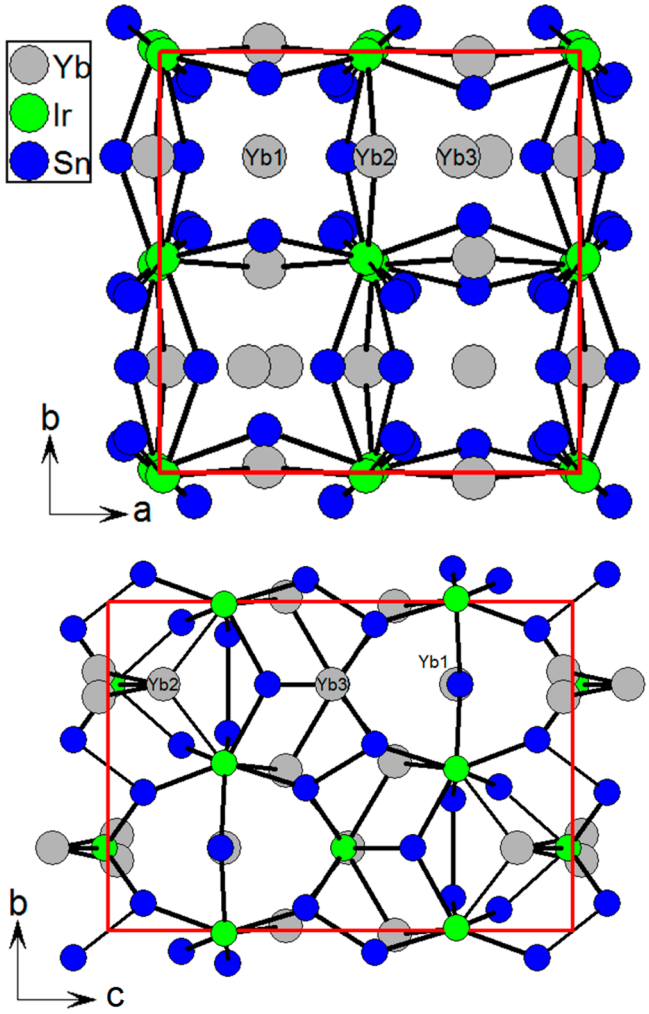

Figure 3. Crystal structure of $Yb_{6.6}Ir_6Sn_{16}$ as viewed along the c-axis (top) and a-axis (bottom). The unit cell is outlined with thick red lines.

factor of the square root of 2 (9.709 × $\sqrt{2}$ = 13.69 Å), $Yb_{6.6}Ir_6Sn_{16}$ and those reported by Cooper are either closely related or they are one and the same. A schematic representation of the relation between the tetragonal $Yb_{6.6}Ir_6Sn_{16}$ and the cubic model (Cooper reported the composition as $Yb_5Ir_{5.5}Sn_{18}$)[11] is shown in Figure 4, and the crystal structures in both symmetries along the c-axis are shown in Figure 5.

dx.doi.org/10.1021/ic500204t | Inorg. Chem. 2014, 53, 6615−6623

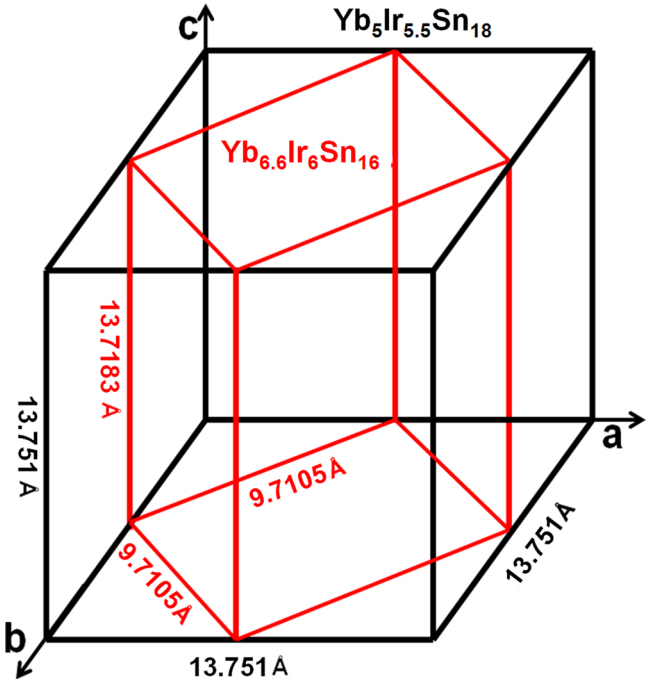

Figure 4. Relationship between the cubic ($Tb_5Rh_6Sn_{17}$) and tetragonal ($Yb_{6.6}Ir_6Sn_{16}$) unit cells.

The crystal structure of $Yb_{6.6}Ir_6Sn_{16}$ in the cubic system has seven crystallographically distinct positions. Two Yb atoms occupy the 16*e* and 4*a* Wyckoff sites with point symmetry 0.3*m* and $\bar{4}3m$, one Ir atom occupies the 24*f* Wyckoff site with point symmetry 2.*mm*, and four Sn atoms occupy 48*h*, 16*e*, 4*c*, and 4*d* Wyckoff sites with point symmetries of ..*m*, 0.3*m*, $\bar{4}3m$, and $\bar{4}3m$, respectively. In the tetragonal system ($Yb_{6.6}Ir_6Sn_{16}$), three distinct Yb atoms occupy Wyckoff positions 2*a*, 8*g*, and 8*g* with point symmetry $\bar{4}m2$, .*m*., and .*m*. One of the 8*g* positions is partially occupied. One Ir and four Sn in the cubic structure rearrange to two Ir atoms occupying the 4*c* and 8*f* Wyckoff sites of point symmetry 2*mm*. and ..2, respectively, and three Sn atoms occupying Wyckoff positions 8*g*, 16*h*, and 8*g* of point symmetry .*m*., 1, and .*m*., respectively. The full stoichiometry of this structure type is $Yb_9Ir_6Sn_{16}$. The fact that the single-crystal refinement gives only $Yb_{6.6}Ir_6Sn_{16}$ suggests a very large number of Yb(3) vacancies in the lattice.

The crystal structures in both compounds ($Yb_5Ir_{5.5}Sn_{18}$ and $Yb_{6.6}Ir_6Sn_{16}$) are closely related to each other in terms of the arrangement of atoms. As shown in Figure 6, both structures are formed by the interconnection of a large cage-type structure made up of 14 Ir atoms and 20 Sn atoms. Both compounds contain Ir_4Sn_4 and Ir_6Sn_{12} units connected through the Ir atoms. Some notable differences between the two structures include that the Sn(3) atom in the cubic system is instead Yb(3) in the tetragonal structure. The Ir atoms split into two atomic sites in the tetragonal system, and a slight distortion in the Ir_4Sn_{12} unit results in the reduction of symmetry from cubic to tetragonal. Ir_4Sn_4 and Ir_4Sn_{12} units are connected through the Ir atoms with two Ir−Sn1 bonds (2.6994 Å and 2.7204(12) Å for $Yb_5Ir_{5.5}Sn_{18}$ and $Yb_{6.6}Ir_6Sn_{16}$, respectively) and two Ir−Sn2 bonds (2.7097 Å and 2.6655(19) Å for $Yb_5Ir_{5.5}Sn_{18}$ and $Yb_{6.6}Ir_6Sn_{16}$, respectively).

The local coordination environments of Yb, Ir, and Sn atoms (within the limiting sphere of 3.6 Å) are presented in Figure 7. The Yb(1) atom is located at the center of a cage consisting of

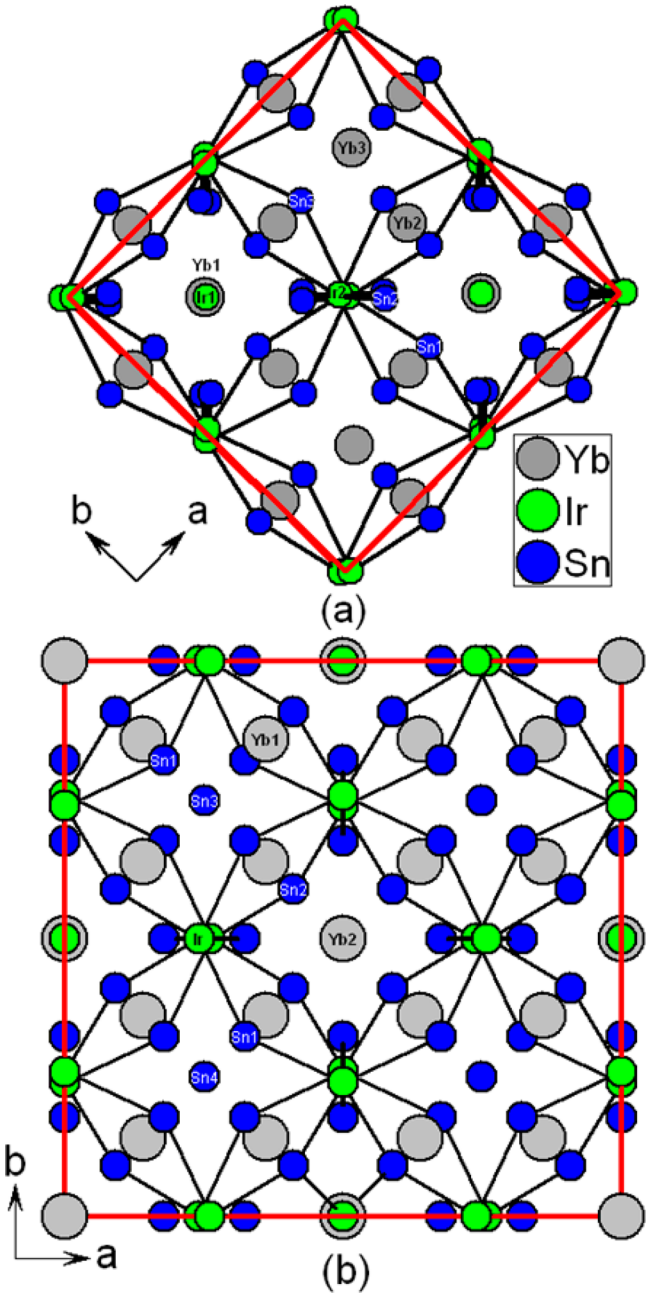

Figure 5. Structural comparison between tetragonal $Yb_{6.6}Ir_6Sn_{16}$ and reported cubic $Yb_5Ir_{5.5}Sn_{18}$ ($Tb_5Rh_6Sn_{17}$ structure type)[11] compounds.

12 Sn and six Ir atoms [$Yb[Sn_{12}Ir_6]$], while the Yb(2) atom is surrounded by three Ir and nine Sn atoms. The disordered atom Yb(3) alternates with vacancies in the lattice and has a coordination environment consisting of seven atoms composed of two Yb and five Sn atoms. The Yb−Ir bond lengths vary from 2.9681(9) to 3.4024(19) Å and Yb−Sn distances are also vary from 3.1825(18) to 3.454(5) Å. The shortest Yb−Ir bond distance of 2.9681(9) Å is normal and comparable to that observed in Yb_2IrGe_2 (2.970 Å).[46] Similarly, the shortest Yb−Sn bond distance 3.1825(18) Å is comparable to the distance in $YbBaSn_3$ (3.153 Å).[46] Interestingly, the Yb(1) atoms are located in much larger cages than other Yb atoms with corresponding Yb(1)−Ir and Yb(1)−Sn average distances of 3.5525 and 3.4001 Å, respectively, suggesting weaker interactions with the Ir and Sn atoms. Both Ir atoms are in

dx.doi.org/10.1021/ic500204t | Inorg. Chem. 2014, 53, 6615−6623

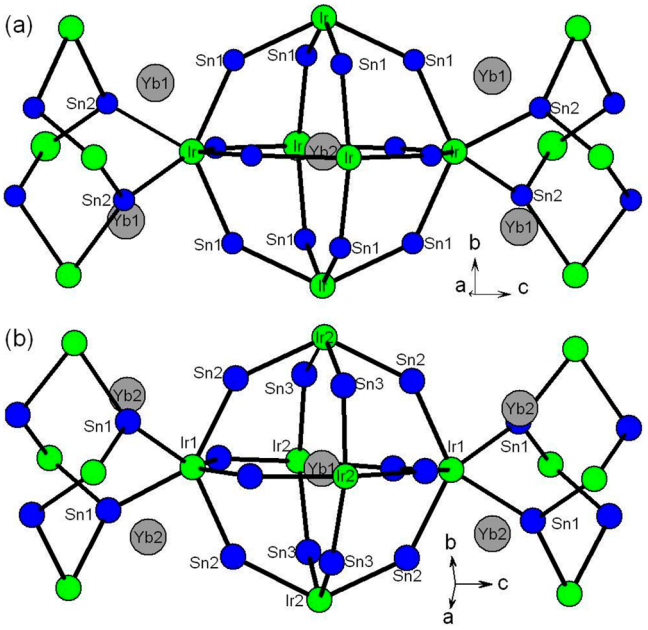

Figure 6. Structural unit comparison in the compounds (a) reported cubic $Yb_5Ir_{5.5}Sn_{18}$[11] and (b) tetragonal $Yb_{6.6}Ir_6Sn_{16}$.

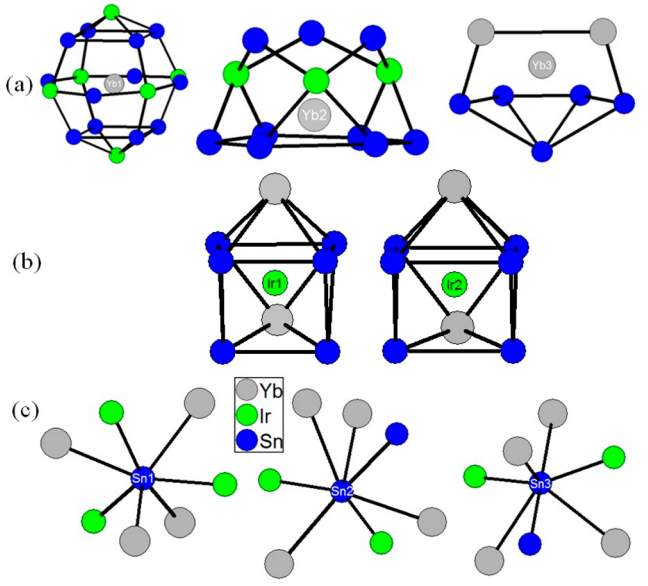

Figure 7. Coordination environment of (a) Yb, (b) Ir, and (c) Sn atoms in the crystal structure of $Yb_{6.6}Ir_6Sn_{16}$.

the same coordination environment of tricapped triangular prism with a coordination number of nine (Figure 7b). The three Sn atoms exist in the tricapped trigonal environment with coordination number of seven as shown in Figure 7c.

3.3. Magnetism. The molar magnetic susceptibility ($\chi_m = M/H$) of $Yb_{6.6}Ir_6Sn_{16}$ measured in a field of 5 kOe is shown in Figure 8. With decreasing temperature, χ_m increases and exhibits no magnetic ordering down to 2 K. The behavior of $\chi_m(T)$ in the temperature range of 75−300 K follows the Curie−Weiss law. The inset of Figure 8 shows the plot of $\chi_m^{-1}(T)$. The straight line passing through the data points is the fit to the Curie−Weiss law with a Weiss constant of −9.5 K. The negative sign indicates predominantly antiferromagnetic interactions. The calculated effective magnetic moment μ_{eff} is

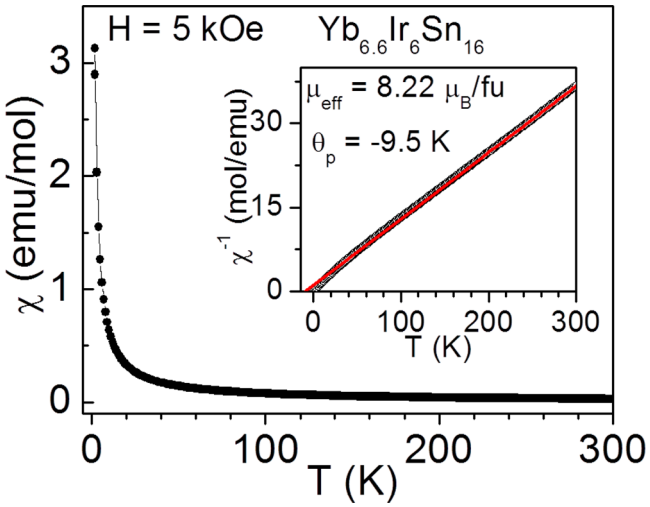

Figure 8. Magnetic susceptibility ($\chi = M/H$) of $Yb_{6.6}Ir_6Sn_{16}$ measured in a field of 5 kOe is plotted as a function of temperature. (inset) Plot of $\chi^{-1}(T)$. The values of paramagnetic Curie temperature (θ_p) and effective Bohr magneton number (μ_{eff}) calculated from the slope and intercept obtained from the linear region of the $\chi^{-1}(T)$ plot are also shown. The magnetic susceptibility can be converted to SI units using the conversion factor of $4\pi \times 10^{-6}$ m^3/mol; the magnetic field strength in oersted can be converted into SI units using the conversion factor of $(10^3/4\pi)$ A/m.

3.21 μ_B/Yb ion (or 8.22 μ_B/fu), which is about 70% of the expected value for a free Yb^{3+} ion (calculated as $\mu_{eff} = gJ[\sqrt{J(J+1)}]$, for $g = 8/7$, $J = 7/2$, $L = 3$, and $S = 1/2$). Assuming that the Ir and Sn atoms do not possess a magnetic moment, the observed magnetism in this compound suggests the presence of mixed-valent Yb atoms.

3.4. X-ray Absorption Near-Edge Spectroscopy. To further probe the Yb valence state in $Yb_{6.6}Ir_6Sn_{16}$, the X-ray absorption measurements were performed at the Yb L_{III} edge, at 300 K and ambient pressure, Figure 9. The main absorption peak (white line resonance) of the spectrum, centered at ~8947.5 eV, is attributed to trivalent Yb atoms.[14,47−49] The spectra also revealed the presence of a weaker feature (shoulder) at ~8939.5 eV, revealing unequivocally that some

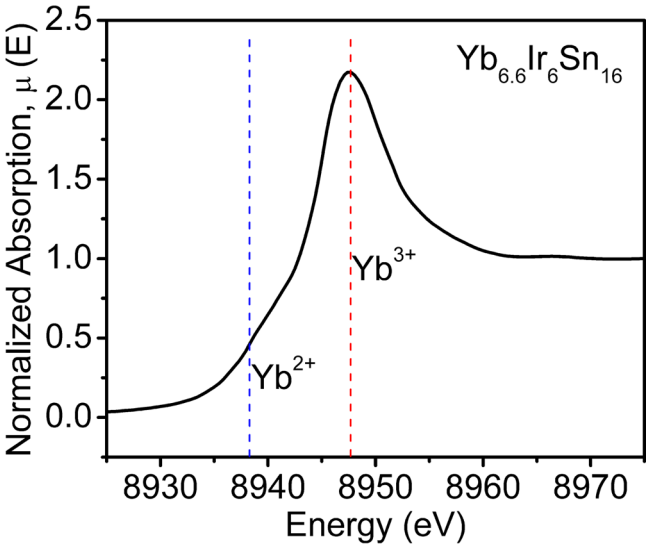

Figure 9. Yb L_{III} absorption edge spectra in $Yb_{6.6}Ir_6Sn_{16}$ at 300 K.

dx.doi.org/10.1021/ic500204t | Inorg. Chem. 2014, 53, 6615−6623

divalent Yb is also present.[14,47−49] Since more than one Yb crystallographic site is present in $Yb_{6.6}Ir_6Sn_{16}$, the compound can be classified as either an intermediate valence compound with all Yb atoms having a noninteger valence or a heterogeneous mixed-valence compound, in which specific Yb atoms are either exactly 2+ or 3+. The relative amounts of the two electronic configurations were estimated by decomposing the normalized Yb XANES into a pair of arctangents (representing the edge step) and Lorentzian functions (representing the white-line resonance).[50] Fitting of the data with the above technique resulted in ∼88% Yb^{3+} and ∼12% Yb^{2+}, which corresponds to an average Yb valence of ∼2.88. Comparison of the real part of the extended X-ray absorption fine structure Fourier transform suggests the possible presence of ∼5% of a Yb^{3+} oxide impurity as well. Because of this oxide impurity, we believe the actual intrinsic valence of Yb in the sample is perhaps closer to 2.80. This value is in reasonable agreement with magnetic measurements. The uncertainty in the absolute valence is ∼5%, arising from correlations between parameters used to represent the edge-step and white-line resonances and from systematic errors due to fitting-model dependence.

3.5. Electrical Resistivity and Heat Capacity. The temperature-dependent resistivity data of a polycrystalline sample of $Yb_{6.6}Ir_6Sn_{16}$ is shown in Figure 10. The resistivity

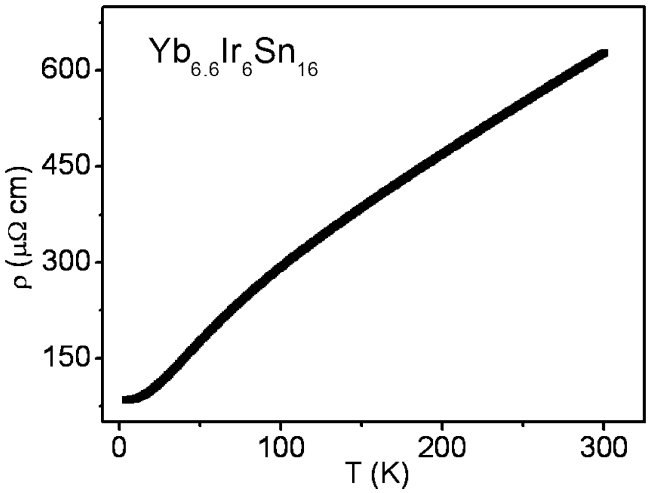

Figure 10. Resistivity (ρ) measured as a function of temperature at zero applied field.

decreases with decreasing temperature, typical for metallic systems.[51] The absolute resistivity value of $Yb_{6.6}Ir_6Sn_{16}$ at 303 K is 650 $\mu\Omega$ cm, which is typical of a poor metal a feature which may be related to strong scattering from the Yb site vacancies in the lattice.

Temperature-dependent heat capacity (C_p) of $Yb_{6.6}Ir_6Sn_{16}$ was measured in the range of 1.8 K < T < 30 K using a commercial Quantum Design Physical Property Measurement System (QD-PPMS). The data were obtained under standard thermal relaxation methods in a zero magnetic field. The temperature-dependent molar specific heat for a $Yb_{6.6}Ir_6Sn_{16}$ sample is shown in Figure 11. Below 7 K, C_p reaches a minimum, and on further reduction in temperature, there is a sudden increase in C_p (which is more clearly seen in the case of C_p/T vs T^2). Assuming the Debye low-temperature approximation, the measured specific heat can be given as

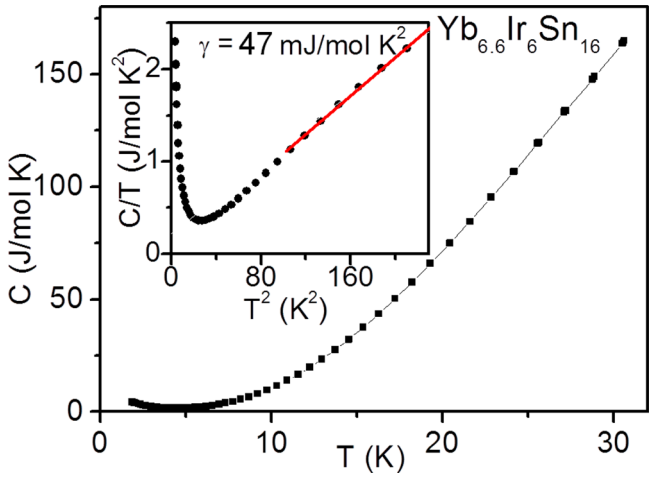

Figure 11. Molar specific heat (C_p) of $Yb_{6.6}Ir_6Sn_{16}$. (inset) Plot of C_p/T vs T^2.

$$C_p = \gamma T + \beta T^3 \quad \text{or} \quad C/T = \gamma + \beta T^2 \tag{1}$$

where γ is the charge carrier contribution also known as Sommerfeld parameter, and β is the lattice contribution. Owing to the upturn in the plot of C/T versus T^2 at lower temperatures, the electronic specific heat capacity coefficient was calculated for a higher temperature range ($100 < T^2 < 200$). The γ value (47 mJ mol^{-1} K^{-2}) obtained from the fitting is low to rule in any heavy Fermion behavior in $Yb_{6.6}Ir_6Sn_{16}$. In the absence of a nonmagnetic counterpart of $Yb_{6.6}Ir_6Sn_{16}$, it was not possible to quantify the magnetic part of the specific heat.

CONCLUDING REMARKS

Well-characterized ternary ytterbium stannides[52−57] and ternary iridium stannides[58,59] are relatively rare, but they form an interesting group of intermetallic compounds that promises to harbor interesting properties. Here we described a ternary Yb−Ir stannide that features mixed valency and strong Yb lattice vacancies and gave a full physical characterization of its properties. Though Espinosa reported[10] the existence of the five different structure types in the tin-rich Yb−Ir−Sn family, the synthesis conditions using the metal flux technique we report here leads to a new composition $Yb_{6.6}Ir_6Sn_{16}$. The compound is tetragonal and closely related to cubic $Yb_5Ir_{5.5}Sn_{18}$. It exhibits mixed valence, which is supported with magnetic susceptibility measurements and XANES. One might expect the existence of other compounds within the same family, which may be achieved by changing the reaction conditions.

ASSOCIATED CONTENT

Supporting Information

Crystallographic information file (CIF). This material is available free of charge via the Internet at http://pubs.acs.org/.

AUTHOR INFORMATION

Corresponding Authors

*E-mail: sebastiancp@jncasr.ac.in. (S.C.P.)
*E-mail: m-kanatzidis@northwestern.edu. (M.G.K.)

Notes

The authors declare no competing financial interest.

dx.doi.org/10.1021/ic500204t | Inorg. Chem. 2014, 53, 6615−6623

■ ACKNOWLEDGMENTS

Financial support from Jawaharlal Nehru Centre for Advanced Scientific Research, Department of Science and Technology (DST) (Grant SR/S2/RJN-24/2010) and Sheikh Saqr Laboratory is gratefully acknowledged. U.S. thanks Council of Scientific and Industrial Research for a research fellowship, and S.C.P. thanks DST for a Ramanujan Fellowship. PNC/XSD facilities and research at these facilities are supported by the U.S. Department of Energy (DOE) and its founding institutions. At Argonne work is supported by the U.S. DOE, Office of Basic Energy Sciences under Contract No. DE-AC02-06CH11357.

■ REFERENCES

(1) Dwight, A. E.; Harper, W. C.; Kimball, C. W. *J. Less-Common Met.* **1973**, *30*, 1−8.
(2) Salamakha, P. S.; Sologub, O. L.; Yakinthos, J. K.; Routsi, Ch. D. *J. Alloys Compd.* **1998**, *265*, L1−L2.
(3) Chevalier, B.; Sebastian, C. P.; Pöttgen, R. *Solid State Sci.* **2006**, *8*, 1000−1008.
(4) Selsane, M.; Lebail, M.; Hamdaoui, N.; Kappler, J. P.; Noël, H.; Achard, J. C.; Godart, C. *Physica B* **1990**, *163*, 213−215.
(5) Pöttgen, R.; Hoffmann, R.-D.; Möller, M. H.; Kotzyba, G.; Künnen, B.; Rosenhahn, C.; Mosel, B. D. *J. Solid State Chem.* **1999**, *145*, 174−181.
(6) François, M.; Venturini, G.; Malaman, B.; Roques, B. *J. Less-Common Met.* **1990**, *160*, 197−213.
(7) Aoki, Y.; Fukuhara, T.; Sugawara, H.; Sato, H. *J. Phys. Soc. Jpn.* **1996**, *65*, 1005−1009.
(8) Niepmann, D.; Pöttgen, R.; Poduska, K. M.; DiSalvo, F. J.; Trill, H.; Mosel, B. D. *Z. Naturforsch. B* **2001**, *56*, 1−8.
(9) Venturini, G.; Malaman, B.; Roques, B. *Mater. Res. Bull.* **1989**, *24*, 1135−1139.
(10) Espinosa, G. P. *Mater. Res. Bull.* **1980**, *15*, 791−798.
(11) Cooper, A. S. *Mater. Res. Bull.* **1980**, *15*, 799−805.
(12) Sebastian, C. P.; Kanatzidis, M. G. *J. Solid State Chem.* **2010**, *183*, 2077−2081.
(13) Sebastian, C. P.; Salvador, J.; Martin, J. B.; Kanatzidis, M. G. *Inorg. Chem.* **2010**, *49*, 10468−10474.
(14) Chondroudi, M.; Peter, S. C.; Malliakas, C. D.; Balasubramanian, M.; Li, Q. A.; Kanatzidis, M. G. *Inorg. Chem.* **2011**, *50*, 1184−1193.
(15) Peter, S. C.; Chondroudi, M.; Malliakas, C. D.; Balasubramanian, M.; Kanatzidis, M. G. *J. Am. Chem. Soc.* **2011**, *133*, 13840−13843.
(16) Disseler, S. M.; Svensson, J. N.; Peter, S. C.; Byers, C. P.; Baines, C.; Amato, A.; Giblin, S. R.; Carretta, P.; Graf, M. J. *Phys. Rev. B* **2011**, *84*, 174429 (1−8).
(17) Peter, S. C.; Rayaprol, S.; Francisco, M. C.; Kanatzidis, M. G. *Eur. J. Inorg. Chem.* **2011**, 3963−3968.
(18) Subbarao, U.; Peter, S. C. *Inorg. Chem.* **2012**, *51*, 6326−6332.
(19) Iyer, A. K.; Peter, S. C. *Eur. J. Inorg. Chem.* **2012**, *33*, 5578−5578.
(20) Peter, S. C.; Disseler, S. M.; Svensson, J. N.; Carretta, P.; Graf, M. J. *J. Alloys Compd.* **2012**, *516*, 126−133.
(21) Sarkar, S.; Peter, S. C. *J. Chem. Sci.* **2012**, *124*, 1385−1390.
(22) Peter, S. C.; Kanatzidis, M. G. *Z. Anorg. Allg. Chem.* **2012**, *638*, 287−293.
(23) Peter, S. C.; Malliakas, C. D.; Nakotte, H.; Kothapilli, K.; Rayaprol, S.; Schultz, A. J.; Kanatzidis, M. G. *J. Solid State Chem.* **2012**, *187*, 200−207.
(24) Peter, S. C.; Sarkar, S.; Kanatzidis, M. G. *Inorg. Chem.* **2012**, *51*, 10793−10799.
(25) Subbarao, U.; Peter, S. C. *Cryst. Growth Des.* **2013**, *13*, 953−959.
(26) Subbarao, U.; Gutmann, M. J.; Peter, S. C. *Inorg. Chem.* **2013**, *52*, 2219−2227.
(27) Subbarao, U.; Peter, S. C. *Adv. Mater. Phys. Chem.* **2013**, *3*, 54−59.
(28) Sarkar, S.; Gutmann, M. J.; Peter, S. C. *CrystEngComm* **2013**, *15*, 8006−8013.
(29) Peter, S. C.; Malliakas, C. D.; Kanatzidis, M. G. *Inorg. Chem.* **2013**, *52*, 4909−4915.
(30) Subbarao, U.; Sarkar, S.; Gudelli, V. K.; Kanchana, V.; Vaitheeswaran, G.; Peter, S. C. *Inorg. Chem.* **2013**, *52*, 13631−13638.
(31) Peter, S. C.; Subbarao, U.; Sarkar, S.; Vaitheeswaran, G.; Svane, A.; Kanatzidis, M. G. *J. Alloys Compd.* **2014**, *589*, 405−411.
(32) Lawrence, J. M.; Chen, Y.-Y.; Thompson, J.; Borges, H. A. *Theoretical and Experimental Aspects of Valence Fluctuations and Heavy Fermions*; Gupta, L. C., Malik, S. K., Eds.; Plenum: New York and London, 1987.
(33) Lawrence, J. M.; Riseborough, P. S.; Parks, R. D. *Rep. Prog. Phys.* **1981**, *44*, 1−85.
(34) Kindler, B.; Finsterbusch, D.; Graf, R.; Ritter, F.; Assmus, W.; Lüthi, B. *Phys. Rev. B* **1994**, *50*, 704(1−4).
(35) Stewart, G. R. *Rev. Mod. Phys.* **2001**, *73*, 797−855.
(36) Pikul, A. P.; Kaczorowski, D.; Bukowski, Z.; Gofryk, K.; Burkhardt, U.; Grin, Yu.; Steglich, F. *Phys. Rev. B* **2006**, *73*, 092406(1−5).
(37) Stewart, G. R. *Rev. Mod. Phys.* **1984**, *56*, 755−787.
(38) Kowalczyk, A.; Falkowski, M.; Toliński, T.; Chełkowska, G. *Solid State Commun.* **2006**, *139*, 5−8.
(39) Jaccard, D.; Wilhelm, H.; Alami-Yadri, K.; Vargoz, E. *Physica B* **1999**, *259*−*261*, 1−7.
(40) Alami-Yadri, K.; Wilhelm, H.; Jaccard, D. *Eur. Phys. J. B* **1998**, *6*, 5−11.
(41) Alami-Yadri, K.; Jaccard, D. *Solid State Commun.* **1996**, *100*, 385−387.
(42) Jaccard, D.; Link, P.; Vargoz, E.; Alami-Yadri, K. *Phys. B* **1997**, *230*, 297−300.
(43) STOE, Cie. In *X-AREA, IPDS Software;* STOE & Cie GmbH: Darmstadt, Germany, 2006.
(44) Petříček, V.; Dušek, M.; Palatinus, L. *Jana2006. The crystallographic computing system;* Institute of Physics: Praha, Czech Republic, 2006.
(45) Vandenberg, J. M. *Mater. Res. Bull.* **1980**, *15*, 835−847.
(46) Rodewald, U. C.; Pöttgen, R. *Solid State Sci.* **2003**, *5*, 487−493.
(47) Rao, C. N. R.; Sarma, D. D.; Sarode, P. R.; Sampathkumaran, E. V.; Gupta, L. C.; Vijayaraghavan, R. *Chem. Phys. Lett.* **1980**, *76*, 413−415.
(48) Hatwar, T. K.; Nayak, R. M.; Padalia, B. D.; Ghatikar, M. N.; Sampathkumaran, E. V.; Gupta, L. C.; Vijayaraghavan, R. *Solid State Commun.* **1980**, *34*, 617−620.
(49) Moreschini, L.; Dallera, C.; Joyce, J. J.; Sarrao, J. L.; Bauer, E. D.; Fritsch, V.; Bobev, S.; Carpene, E.; Huotari, S.; Vankó, G.; Monaco, G.; Lacovig, P.; Panaccione, G.; Fondacaro, A.; Paolicelli, G.; Torelli, P.; Grioni, M. *Phys. Rev. B* **2007**, *75*, 035113(1−8).
(50) Chondroudi, M.; Balasubramanian, M.; Welp, U.; Kwok, W. K.; Kanatzidis, M. G. *Chem. Mater.* **2007**, *19*, 4769−4775.
(51) Dremov, R. V.; Koblyuk, N.; Mudryk, Ya.; Romaka, L.; Sechovský, V. *J. Alloys Compd.* **2001**, *317*, 293−296.
(52) Beyermann, W. P.; Hundley, M. F.; Canfield, P. C.; Thompson, J. D.; Latroche, M.; Godart, C.; Selsane, M.; Fisk, Z.; Smith, J. L. *Phys. Rev. B* **1991**, *43*, 13130(1−7).
(53) Fornasini, M. L.; Manfrinetti, P.; Mazzone, D. *Z. Kristallogr.—New Cryst. Struct.* **2010**, *225*, 221−222.
(54) Fornasini, M. L.; Manfrinetti, P.; Mazzone, D.; Riani, P.; Zanicchi, G. *J. Solid State Chem.* **2004**, *177*, 1919−1924.
(55) Fornasini, M. L.; Zanicchi, G.; Mazzone, D.; Riani, P. *Z. Kristallogr.—New Cryst. Struct.* **2001**, *216*, 21−22.
(56) Lei, X. W.; Zhong, G. H.; Li, M. J.; Mao, J. G. *J. Solid State Chem.* **2008**, *181*, 2448−2455.
(57) Schmitt, D. C.; Haldolaarachchige, N.; Young, D. P.; Jin, R. Y.; Chan, J. Y. *Z. Anorg. Allg. Chem.* **2011**, *637*, 2046−2051.
(58) Hoffmann, R.-D.; Kussmann, D.; Pöttgen, R. *Int. J. Inorg. Mater.* **2000**, *2*, 135−141.

(59) Wu, Z. Y.; Hoffmann, R.-D.; Pöttgen, R. *Z. Anorg. Allg. Chem.* **2002**, *628*, 1484−1488.